

# The radio emitting X-ray binary systems LS 1+61°303 and Cygnus X-3

Marta Peracaula i Bosch

**ADVERTIMENT.** La consulta d'aquesta tesi queda condicionada a l'acceptació de les següents condicions d'ús: La difusió d'aquesta tesi per mitjà del servei TDX ([www.tesisenxarxa.net](http://www.tesisenxarxa.net)) ha estat autoritzada pels titulars dels drets de propietat intel·lectual únicament per a usos privats emmarcats en activitats d'investigació i docència. No s'autoritza la seva reproducció amb finalitats de lucre ni la seva difusió i posada a disposició des d'un lloc aliè al servei TDX. No s'autoritza la presentació del seu contingut en una finestra o marc aliè a TDX (framing). Aquesta reserva de drets afecta tant al resum de presentació de la tesi com als seus continguts. En la utilització o cita de parts de la tesi és obligat indicar el nom de la persona autora.

**ADVERTENCIA.** La consulta de esta tesis queda condicionada a la aceptación de las siguientes condiciones de uso: La difusión de esta tesis por medio del servicio TDR ([www.tesisenred.net](http://www.tesisenred.net)) ha sido autorizada por los titulares de los derechos de propiedad intelectual únicamente para usos privados enmarcados en actividades de investigación y docencia. No se autoriza su reproducción con finalidades de lucro ni su difusión y puesta a disposición desde un sitio ajeno al servicio TDR. No se autoriza la presentación de su contenido en una ventana o marco ajeno a TDR (framing). Esta reserva de derechos afecta tanto al resumen de presentación de la tesis como a sus contenidos. En la utilización o cita de partes de la tesis es obligado indicar el nombre de la persona autora.

**WARNING.** On having consulted this thesis you're accepting the following use conditions: Spreading this thesis by the TDX ([www.tesisenxarxa.net](http://www.tesisenxarxa.net)) service has been authorized by the titular of the intellectual property rights only for private uses placed in investigation and teaching activities. Reproduction with lucrative aims is not authorized neither its spreading and availability from a site foreign to the TDX service. Introducing its content in a window or frame foreign to the TDX service is not authorized (framing). This rights affect to the presentation summary of the thesis as well as to its contents. In the using or citation of parts of the thesis it's obliged to indicate the name of the author.



**Part III**

**SEARCH FOR PERIODIC BEHAVIOUR  
IN THE RADIO AND X-RAY  
LIGHT CURVES**



## Chapter 7

# Brief introduction to periodicity analysis methods

There are several standard methods to analyse data regularly distributed in time, most of them based in the Fourier analysis. Unfortunately, astronomical observations do not allow to obtain data with such a regularity, since they depend on the telescope time schedules, the position of the object we need to observe and on the weather conditions during the observing run. Thus, even during a given run the data is seldomly evenly distributed in time. Experience shows that interpolation between real data points to produce an even net does not produce good results. The data are usually grouped in temporal clumps, since between two consecutive observational runs several days or months are elapsed, which means several times the periodic cycle. False points introduced by the interpolation procedure are often more frequent than the real ones.

An additional uncertainty, affecting both evenly and unevenly distributed data, is the introduction of fictitious periodicities due to the finite and discrete nature of sampling data. Any sample can be considered as the product of a continuous signal by a fictitious continuous function, whose value is only different than zero in the position of the sample points. This function is called window function. From the convolution theorem, the Fourier spectrum of the product of the signal by the window function is equivalent to the convolution product of the respective Fourier spectra. This means that the Fourier spectrum will be affected (convolutioned) by the window spectrum. The window itself has periodic characteristics that will mix

with those of the data.

These consideration must be taken into account when choosing a method to be applied to a given data distribution.

In the current chapter we briefly present three statistical methods for the detection of periodicities in weak and noisy signals. They can be applied to data unevenly distributed in time, so no interpolated points are needed. They consider the fictitious frequencies introduced by the sampling windows, or the statistical significance of a peak in the power spectrum is analysed.

## 7.1 Fourier Analysis

The standard method used for determining periodicities in the physical signals is the analysis of the Fourier Transform power spectrum of the time-signal function. Let us see the reason for this adoption.

Let us consider a function  $f(t)$ ; if  $f$  is continuous, derivable and convergent in the point  $t$ , it can be decomposed in the following way:

$$f(t) = \int_{-\text{inf}}^{\text{inf}} F(\nu) e^{i2\pi\nu t} d\nu \quad (7.1.1)$$

where

$$F(\nu) = \frac{1}{2\pi} \int_{-\text{inf}}^{\text{inf}} f(x) e^{-i2\pi\nu x} dx \quad (7.1.2)$$

$F(\nu)$  is called Fourier Transform of  $f(t)$ , or, equivalently,  $f(t)$  is the Invers Fourier Transform of  $F(\nu)$ . The functions  $e^{i2\pi\nu t}$  are harmonic functions, whereas  $F(\nu)$  are complex weights, i.e.  $F(\nu) = A(\nu)e^{i\phi(\nu)}$ , where  $A(\nu)$  is the amplitude and  $\phi(\nu)$  the phase.

Hence,  $f(t)$  can be expressed as the sum (integral) of harmonic functions, each of them with its own amplitude and phase. The frequency of this harmonic functions is  $\nu$ . If there is a frequency  $\mu$  such that  $A(\mu) \gg A(\nu)$  for any  $\nu$ , then the harmonic function with this frequency dominates over the sum of the rest of them. In this case  $f(t)$  will have a periodicity highly dominated by the period  $1/\mu$ . The real function

$A(\nu)^2 = |F(\nu)|^2$  is called power spectrum, and it is normally used to highlight the dominant frequencies.

Since in the real physical experiments we deal with discrete data samples, instead of continuous functions, it is necessary to use the discrete Fourier Transform, defined as

$$f(t_r) = f_r = \sum_{k=0}^{N-1} F_k e^{i2\pi\nu_k t_r} \quad (7.1.3)$$

where

$$F(\nu_k) = F_k = \sum_{r=0}^{N-1} f_r e^{-i2\pi\nu_k t_r} \quad (7.1.4)$$

$N$  is the number of points in the sample and  $T$  the time range of the where the data spans.

One of the usual problems of using the Discrete Fourier Transform is the so called 'spectral leakage': peaks can appear in frequencies that not correspond to the harmonical function, mainly due to the finite and discrete sample. It can get emphasized when there are clumps of uniformly separated points. Normally, in order to solve the leakage problem the spectrum is convolved with a smoothing window function, which reduces the variance.

Let  $f(t)$  be a time continuous function describing the real source magnitude and  $F(\nu)$  its Fourier Transform or spectrum. The observed magnitude  $f_s(t)$  can be considered as the product of  $f(t)$  by a sampling function  $s(t)$  accounting by the discrete nature of the observational data, i.e.

$$f_s(t) \equiv f(t)s(t) = \frac{1}{N} \sum_{r=1}^N f(t) \delta(t - t_r) = \frac{1}{N} \sum_{r=1}^N f_r \delta(t - t_r) \quad (7.1.5)$$

(here every point is equally weighted). Since we are interested in finding the FT of  $f(t)$ , i.e.  $F(\nu)$ , the convolution theorem must be applied to equation 7.1.5,

$$D(\nu) = F(\nu) \otimes W(\nu) \quad (7.1.6)$$

where  $D(\nu)$  (dirty spectrum) and  $W(\nu)$  (window function) denote the Fourier Transform of the sampling signal,  $FT[f_s]$ , and spectral window function,  $FT[s]$ , respectively.

Although the Dirty spectrum and the window function are directly computable from the data a solution of equation 7.1.6 from convolution theorem,

$$F(\nu) = FT[f] = FT[f_s/s] = FT[f_s] \otimes FT[1/s] \quad (7.1.7)$$

is not possible, since  $s(t)$  is equal to zero in almost all its domain.

## 7.2 CLEAN algorithm

This is a spectrum analysis method of time series specially useful in case of dealing with data unevenly distributed in time. It is based in a unidimensional complex version of the deconvolution algorithm CLEAN, widely used in bidimensional reconstruction of images (adapted to time series analysis by Roberts et al. 1987), which we have been applying to obtain source maps in the previous chapters. As in the case of maps, in the time series we want to “clean” the dirty spectrum by eliminating the false features.

CLEAN does it by subtracting from the dirty spectrum the expected response of a function composed of a unique harmonical function (as in the case of the maps when the response of a centered point is subtracted). In this way a residual spectrum is produced, where an harmonical function and fake features have been removed. This process is iterated performing successive ‘residual spectra’ until only noise and the ‘spectral clean components’ are left.

When the spectral clean components have been determined they are convolved with a ‘clean beam’ that produces the resolution of the frequency to be about  $1/T$ . It is normally a gaussian normalized in such way that  $B(0)=1$  and equivalent to  $W$  in the central peak. To maintain the noise level the residual spectrum is added to the cleaned one.



## 7.3 Phase dispersion minimization method

Developed by Stellingwerf (1978), this method is based in the idea of selecting the period that yields the minimum observational dispersion with respect to the mean light curve.

We define  $f_i$  as the magnitude observed at the time  $t_i$  and  $N$  the total number of observed points ( $i = 1, \dots, N$ ), then variance of the set is defined as:

$$\sigma^2 = \frac{\sum_{i=1}^{N-1} (f_i - \bar{f})^2}{N-1} \quad (7.3.1)$$

where  $\bar{f} = \frac{\sum_i f_i}{N}$ .

Let us suppose now that we have grouped these data in  $M$  different samples containing  $n_j$  points and a variance  $s_j^2$  ( $j = 1, \dots, M$ ). The total variance,  $s^2$ , is defined as the weighted mean of all individual variances, i.e.

$$s^2 = \frac{\sum_{j=1}^M (n_j - 1) s_j^2}{\sum_{j=1}^M n_j - M} \quad (7.3.2)$$

The method here developed is based on the minimization of the variance with respect to the mean light curve. We define  $\pi$  as the trial period and the phase  $\phi_i$  as  $\phi_i = \frac{t_i}{\pi} - \left[ \frac{t_i}{\pi} \right]$ , where brackets indicate that the integer part of a number is taken.  $M$  subsamples of the sample  $f_i$  are selected so that all the members in the subsample  $j$  have a similar phase. The whole phase interval (0,1) is usually divided in fixed phase beams. All the points  $(f_i, t_i)$  belonging to one of these beams constitute one of these subsamples. The mean light curve is defined as the mean of the  $f_i$  that fall in a common subsample  $j$  ( $j = 1, \dots, M$ ). The total variance,  $s^2$ , measures the total dispersion around the mean light curve.

Let us define the function  $\theta$  as:

$$\theta = \frac{s^2}{\sigma^2} \quad (7.3.3)$$

If  $\pi$  is not a real period, then  $\theta \simeq 1$ ; otherwise, if  $\pi$  is a true period then  $\theta$  will adopt a minimum value, tending to zero in best cases.

This technic, called *Phase Dispersion Minimization Method* (PDM), is actually a ‘Fouriergrama’ of order infinite, since all the harmonics are included in the fitted function. The Fourier Series development often requires additional limitations, and a high order in the serie for non-sinusoidal variations.

Thought individual samples can be selected in many ways, it is convenient to define the beam structure in a standard fashion. The unit phase interval is divided in  $N_b$  equal parts, and each of these parts is also divided in  $N_c$  subdivisions. The individual variances  $s_j$  are found by shifting a beam of length  $\frac{1}{N_b}$  over the whole phase interval, so that all the points found in this beam are considered in the determination of the variance. The shift applied to the beam to determine the next variance will be a phase interval  $\frac{1}{N_b N_c}$ . In this way we will obtain  $M = N_b N_c$  beams of length  $\frac{1}{N_b}$  each, for which we know their individual variance. Boundary conditions on the unit interval have to be considered to obtain a uniform covering.

The curve  $\theta(\pi)$  is calculated for for a given interval of periods  $(\pi_1, \pi_2)$  and with a given resolution between the periods  $\pi$ . Som of the minimums it will show may correspond to real periods. It can be demonstrated that the shape of a minimum approaches to a parabola.

PDM technic finds all the periodic components, so the subharmonics  $\nu_n = \nu_1/n$  ( $\nu_1$  is the main frequency) will also be found. Subharmonics can be detected in three different ways:

1. from the multiple folded shape of the light curve;
2. from the width of the minimums –which are narrower for the subharmonics with increasing  $n$  when we compute the method in the frequency space–;
3. subharmonics reduce their significance when increasing the beam size.

This method is specially useful in case of having few observations performed in a limited range of time, in particular when light curve is clearly non-sinusoidal. PDM

provides us with a good approximation to the light curve from the observational data, from which other periodicity studies can be performed.

## 7.4 Period improving from cross correlation in the phase space

In case of having individual light curves of a source obtained during independent and separated sessions, once a rough signal period has been found by means of any of the previous methods described in the present chapter, a method to determine more accurately the period can be applied, which is more oriented to emphasize the profile repetition than the light curve amplitude (Bendat & Piersol 1971, Taylor & Gregory 1982). This method uses the cross correlation for even data.

If the signal has a periodicity in the range  $(P_0, P_f)$  and we want to determine this period within a resolution  $\delta P$ , then for each  $P = P_0 + k\delta P$  ( $P < P_f$ ) we follow the next steps: First, we must define each individual cycle in the phase space of the period  $P$ . The unit phase interval is then divided in beams of a given width. A mean light curve is defined by averaging all points from different cycles that are in the same beam. Next step consists in correlating each individual cycle with the mean light curve in the phase space. The phase corresponding to a peak in the cross correlation curve will be a measure of the phase difference between the mean and individual light curves -for the real period this phase difference must be zero in all the individual curves. When the standard deviation RMS of each resulting phase is represented as a function of the period the real period is easily identified as that corresponding to a minimum RMS.



# Bibliografy

- [1] Roberts D.H., 1995, IAU Circ. 6269
- [2] Stellingwerf R.F., 1978, ApJ, 224, 953
- [3] Taylor A.R., Gregory P.C. 1982, ApJ, 255, 210 (TG82)
- [4] Taylor A.R., Gregory P.C. 1984, ApJ, 283, 273 (TG84)



## Chapter 8

# The LS I+61°303 periodic strong radio outbursts

### 8.1 Introduction

Soon after LS I+61°303 was discovered to emit in radio wavelengths the source was found to show strong radio outburst that repeat approximately every 26.5 days (Taylor & Gregory, 1982 -hereafter TG82-). A similar modulation observed in the radial velocity derived from its emission lines (Hutchings & Crampton, 1981) seemed to indicate this period to be associated with the orbital motion of the binary. In the past years modulations near 26 days have been also seen in the optical and infrared spectral domains (Mendelson & Mazeh, 1994, and Paredes et al, 1994, respectively). and very recently a periodic variation of approximately 26.7 days has been detected in the X-ray emission from the source (Paredes et al. 1997, this work Chapter 9).

The outbursting radio behavior of LS I+61°303 have been fairly monitored since its discovery. Typical radio outburst are shown in Figure 8.1. In it the labels of the top horizontal axis indicate the radio phase<sup>a</sup> of the source at the corresponding date. The phase origin was set by TG82 at JD 2443366.775, and the period we will usually use to plot or refer to a LS I+61°303 cycle, unless another one is specified, is 26.496 days (determined by Taylor & Gregory, 1984, hereafter TG84 **B**).

---

<sup>a</sup>also referred as orbital phase

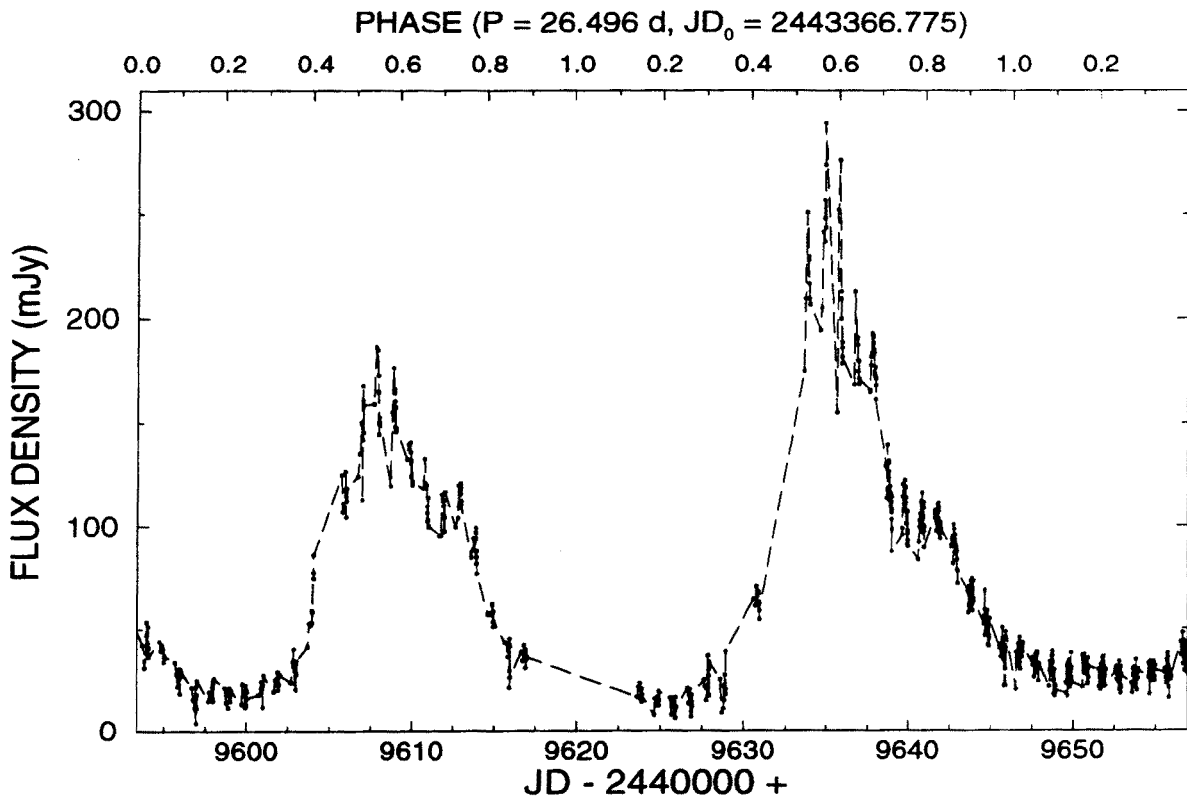


Figure 8.1: Example of two consecutive radio outburst of LS I+61°303 from 8.3 GHz GBI observations.

In spite of the regularity of the radio activity events, individual outbursts differ from each other in their peak intensity and light curve profile. The maximum flux density of the flares ranges from about 60 mJy to 300 mJy (see Figure 8.2), . Furthermore, the phase where the outburst peak varies from cycle to cycle. Strong outburst seem to peak near phase 0.6, whereas lower outbursts have been seen to reach their maximum in the phase range 0.4–1.0 (Paredes et al. 1989 C). This variation in the strength of the outbursts has been proposed to be driven by a long-term time modulation approximately 4 years by Gregory et al. (1989) D and Paredes et al. (1990). A value of  $1600 \pm 30$  days for the period of this long term modulation has been calculated in Estalella et al. (1993 F). On the basis of their extensive radio monitoring with the GBI<sup>b</sup> during 1.5 years, Ray et al. (1996 E) suggest that this modulation could be quasi-periodic or an envelope to the outburst maxima.

We can see in Figure 8.1 that generally radio outbursts have a rapid increase (of the order of 2 days), reach the maximum, and then return back to quiescence

<sup>b</sup>NRAO Green Bank Interferometer



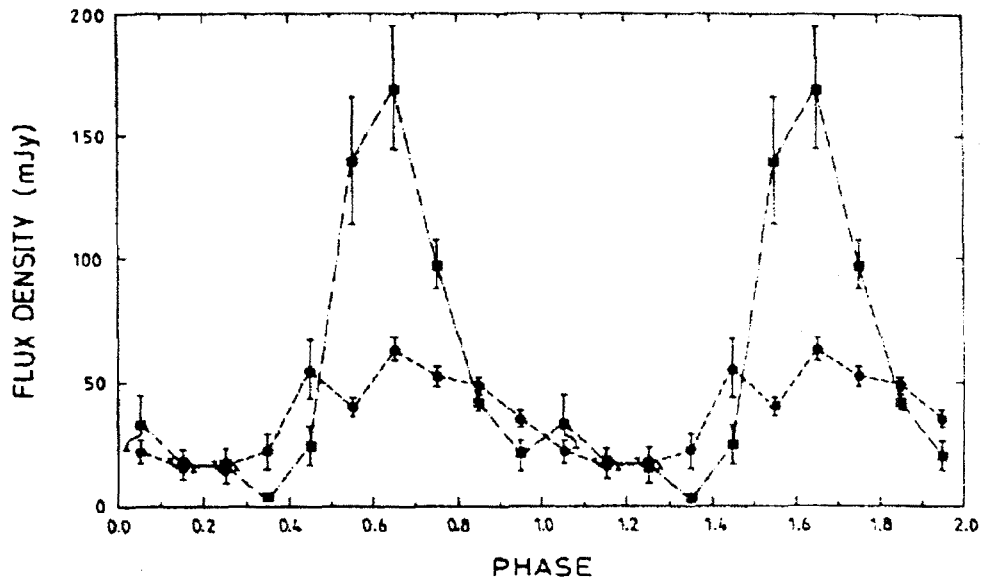


Figure 8.2: Average radio light curves for strong radio outbursts (filled squares) and low radio outbursts (filled circles). Figure reproduced from Paredes et al. 1990.

in a more slowly decay. The time amplitude of the light curve at a flux density level of about half of the peak is approximately 10 days. Nonetheless, we want to remark that outbursts behaving in different ways have been seen, like for example with slower increase rate. The cycles plotted in this figure also show the pattern of an outburst light curve curve is rather complex. They usually seem to be formed by series of smaller flares overlapped to the general trend of the flux density. We refer to them as ‘mini-flares’ or ‘mini-outbursts’. Mini-flares are seen both in the quiescent and active states. An added complication is that many outburst can be multiply peaked, which difficults the establishment a concrete phase for the flare maximum and decreases the reachable accuracy of a period search.

From the existing information about the LS I+61°303 outbursts temporal behaviour we think the following points are noteworthy:

- a) The LS I+61°303~ 26.5 d. period has not been revised since its determination in 1984 (TG84). Much more data is available at this moment.
- b) Variations in the phase of the peak are sometimes very sudden and its relation with the strength of the outburst is not yet totally confirmed. Outburst were suspected to onset at the periastron passage, and therefore a rather constant

phase of the orbital cycle where they reach the maximum flux density was expected. The fact that different flares have been seen to peak at different phases (from 0.4 to 1) is intriguing.

- c) In figure Figure 8.3 we reproduce from Martí (1993 G) the latest reported fit to the suspected  $\sim 4$  years modulation of the outbursts strength. The plotted points are the observed outbursts peak flux density from 1997 to 1993. As it can be seen, there are many gaps between the different cycles observed and many of the plotted data points are lower limits to the outburst maxima (the ones marked with an arrow).

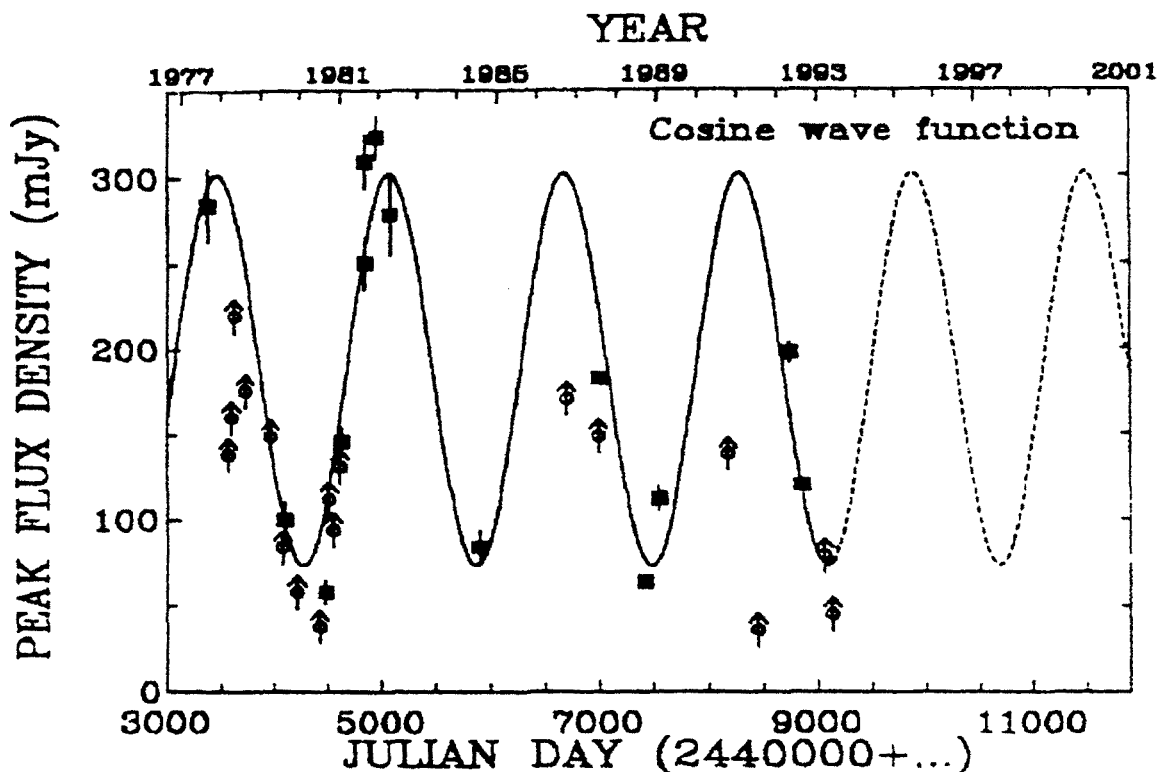


Figure 8.3: Radio outburst peak flux density as a function of Julian date and year. Lower limits on outburst maxima are marked with an arrow. The thick line is the best fit cosine wave function. Reproduced from Martí 1993.

We therefore, initiated a campaign to collect the larger number of LS I+61°303 observations available from different sources: reported in the literature, from collaborators, and the sets our research group have been observing during the previous years. The final data file in 1994 contained 525 data points. In Table 8.1 we indicate

Table 8.1: Summary of the sources of our LS I+61°303 data base file

Reference	Frequency (GHz)	Number of data points	Observing dates
Taylor and Gregory (1982)	5 and 10	143	Aug 1977–Mar 1981
Taylor and Gregory (1984)	5 and 10	28	Aug 1981–Sep 1981
Gregory et al. (1989)	5	29	Jul 1984–Sep 1986
Nelson (1989)	5	139	Jun 1987–Aug 1987
Paredes et al. (1990)	8.4	34	Sep 1988–Jan 1989
Paredes et al. (1990)	8.4	34	Sep 1988–Jan 1989
Own data. DSN (Madrid, INTA-NASA)	8.4	23	Oct 1990–May 1992
VLBI data (VLA June, 1992)	5	42	Jun 1992–Jun 1992
VLA (August 1992)	5 and 1.5	21	Aug 1992–Sep 1992
Own data. DSN (INTA-NASA)	8.4	41	Feb 1993–May 1993
Own data. DSN (INTA-NASA)	8.4	25	Apr 1994–May 1995

the sources of these LS I+61°303 data sets, frequency of the observations, Julian Date range of the sets, and number of points of each data set.

In 1995 we established a collaborative relation Paul Ray, Elizabeth Waltman and Roger Foster<sup>c</sup> which had been daily monitoring LS I+61°303 at 8.3 GHz and 2.25 GHz since January 1994 with the Green Bank Interferometer. As a result of it the LS I+61°303 data file we had been collected and the GBI 8.3 GHz data points monitored from January 1994 to February 1996 were joined. The GBI data represented 6566 new points in the data file, all at the same frequency, and spanned in only two years.

The resulting data base of LS I+61°303 radio observations from 1978 to 1996 has been used for the period analysis of the radio emission from source we describe in the next sections.

<sup>c</sup>Remote Sensing Division, Naval Research Laboratory

Table 8.2: Summary of the periodicity search results obtained for the data reported in TG82 -that was obtained from 1977 to 1981- and the 8.3 GHz GBI data obtained from 1994 to 1996.

Method	GBI-95 data (days)	TG-82 data (days)
CLEAN	$26.70 \pm 0.07$	$26.46 \pm 0.07$
PDM	$26.75 \pm 0.06$	$26.46 \pm 0.04$
CC ("TG82 method")	$26.78 \pm 0.04$	$26.52 \pm 0.04$

## 8.2 Periodicity analysis of the LS I+61°303 radio outburst

We applied the CLEAN and PDM algorithm for periodic signal analysis to two subsets of our data base: a) The data reported in TG82 taken from 1977 to 1981 and b) the 8.3 GHz GBI data obtained from 1994 to 1996, partly reported in Ray et al. 1996.

The results of both subsets are shown in Figures 8.4 and 8.5 for the CLEAN algorithm and the PDM method respectively, and reported in Table 8.2.

The immediate result is that we obtain for the data of TG82 exactly the same results obtained by this authors, with different period search methods than the applied by them. However for the more modern data from the GBI the period obtained with the same algorithms is about 26.7 days.

We think this is very probably indicative of a change in the period of LS I+61°303 in the about 14 years from the average of the epoch ranges of the two subsets.

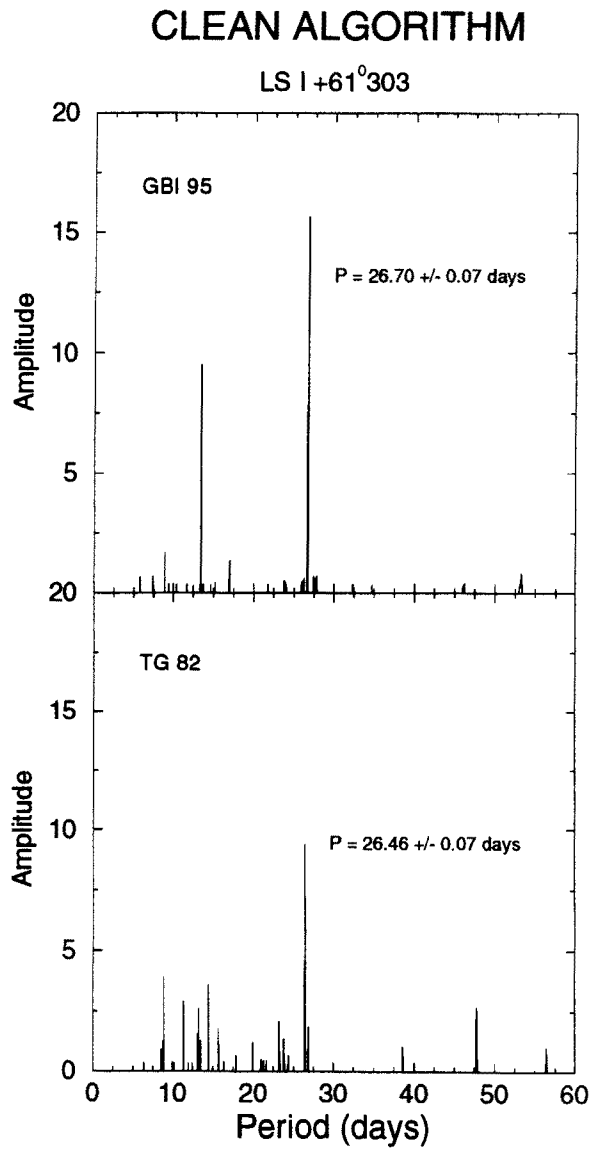


Figure 8.4: Clean spectrum obtained for the 1994-1996 8.3 GHz data (top panel) and the TG82 1979-1981 data (bottom panel) respectively.

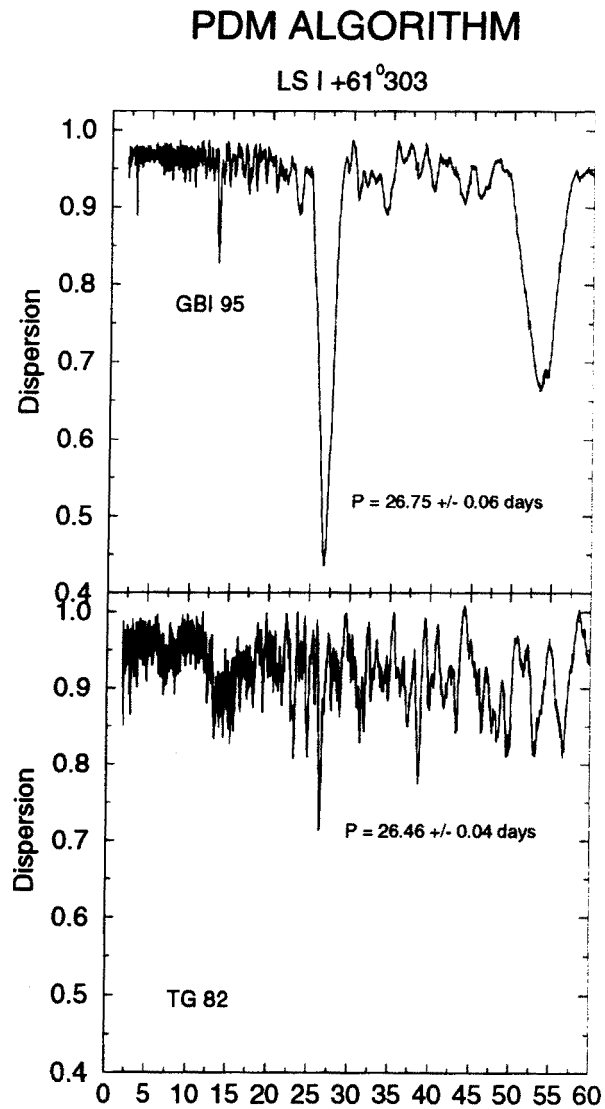


Figure 8.5: Periodogram obtained for the 1994-1996 8.3 GHz data (top panel) and the TG82 1979-1981 data (bottom panel) respectively using the phase dispersion minimization technique (PDM).

# Bibliografy

- [1] Estalella R., Paredes J.M., Rius A., Martí J., Peracaula M.. 1993, A&A, 268, 178
- [2] Gregory P.C., Taylor A.R., Crampton D., Hutchings J.B., Hjellming R.M., et al., 1979, AJ, 84, 1030
- [3] Gregory P.C., Huang-Jian Xu, Backhouse C.J., Reid, A. 1989, ApJ, 339, 1054
- [4] Hutchings, J.B., Crampton, D. 1981, PASP 93, 486
- [5] Martí, J. 1993, PhD thesis, University of Barcelona
- [6] Mendelson, H., Mazeh, T. 1989, MNRAS, 239, 733
- [7] Paredes, J.M., Estalella, R., Rius, A. 1990, A&A, 232, 377
- [8] Paredes, J.M., Marziani, P., Martí, J., Fabregat, J., Coe, M.J., et al., 1994, A&A, 288, 519
- [9] Paredes, J.M., Martí, J., Peracaula, M., Ribó, M. 1997, A&A, 320, L25
- [10] Ray, P.S., Foster, R.S., Waltman, E.B., Ghigo, F.D., Johnston, K.J. 1996, in /it Radio Emission from the Stars and the Sun, ASP Conference Series. Vol. 93, p. 248, A.R. Taylor and J.M. Paredes (eds.)
- [11] Taylor A.R., Gregory P.C. 1982, ApJ, 255, 210 (TG82)
- [12] Taylor A.R., Gregory P.C. 1984, ApJ, 283, 273 (TG84)





# Chapter 9

## Short term radio variability of LS I+61°303

### 9.1 Introduction

Even though at a first glance the radio light curves of LS I+61°303 seem to consist in a simple repetitive pattern (strong periodic outbursts that peak every 26.5 days), a close look to each one of the individual flares reveal a rather complex structure in their profile. As we have already mentioned in different parts of this work, small amplitude flares overlapped onto the general trend of the radio curves are clearly perceived. The time scale of their rise and decay usually is of the order of hours ( $\sim 6\text{--}12\text{h}$ ), and the flux density variation is of the order of tens of mJy ( $\sim 20\text{--}50$  mJy). They have been seen both in the quiescent and the active states of LS I+61°303 radio emission and don't seem to show a concrete sequence in the individual cyclic outflows. We refer to this low amplitude bursts as '**mini-flares**'.

Up to this moment very few high timing resolution radio light curves of LS I+61°303 had been obtained. In our VLA data presented in Chapter 5 we dispose of a data point every 30 seconds. In them we have noticed that, in addition to mini-flares, series of very low flux density bumps or 'jumps' are occasionally slightly discernible. We refer to this very low amplitude burst as '**micro-flares**'. Previous LS I+61°303 radio photometry (with  $\sim 10$  minute resolution) was published by Gregory et al. (1979) and Taylor and Gregory (1984), here after TG84. These

authors reported significant flux density variations in time scales from a few hours to as short as 30 minutes. According to TG84, these details in the LS I+61°303 radio light curve can be accounted for by episodic events of relativistic particle production due to luminosity-driven shocks (LDSs). In the context of supercritical accretion models, the LDSs should occur around the periastron passage of a highly eccentric orbit, when the radiation pressure of the normal star increases up to the Eddington limit and a blast wave sweeps away the amount of matter in excess of the critical accretion rate. A similar model has been proposed by Haynes et al. (1980) for the periodic radio outbursts of the REXRB Cir X-1.

In particular, TG84 point out that the outburst flux density rise reported by Gregory et al. (1979) was observed to consist of particle injection episodes. They attributed them to consecutive LDSs with a duration of a few  $10^3$  s and with a remarkably repeatable separation interval of  $\sim 10^5$  s. Each LDS episode caused a 6 cm flux density increase of a few tens of mJy. The combined effect of several LDSs may lead to the formation of a large ionized plasma cloud or plasmon. This plasmon containing shock-accelerated relativistic electrons will later expand, accounting for the time and spectral evolution of the strong periodic LS I+61°303 radio outbursts, as modeled by Paredes et al. (1991). It is important to point out here that the separation interval between shocks is interpreted as the free fall time of the accreted matter from the periastron separation. TG84 also find that the shock clears the volume between the binary components in a time scale safely shorter than the shock interval, so that the next blast can take place, consistently with their picture.

Since a better knowledge of the temporal behaviour of the synchrotron emission can help to understand the provenience of the relativistic particles that originate it, our purpose in this chapter is to further study the short term time variation of LS I+61°303 radio brightness. We present here the analysis we carried out of the radio variability at short scales of this source over a total time span of more than 30 hours split into three different, non-consecutive observing days.

## 9.2 Observations and data reduction

We used the observations presented in Chapter 5, taken with the VLA at 6 cm on June 6 1990, and September 9 and 13 1993. The details on the observation and calibration procedures have already been described in that chapter, as well as the

Table 9.1: Date and LS I+61°303 radio phase of the observing sessions

Date	Julian Date 2440000.0 +	Radio phase (P = 26.496 days) (t0 = 2443366.775 )
1990 June 6	8049.0	0.72
1993 September 9	9239.8	0.66
1993 September 13	9243.8	0.81

configuration and the calibrators used for the observations.

In Table 9.1 we have listed the radio phase of LS I+61°303 for each of the observing sessions according to the radio period and phase origin of TG84. We remind here that in all these dates the VLA was participating as an interferometer element in VLBI experiments, although since we also dispose of the usual array data output we are able to use them for this analysis.

The plots in Figure 9.1 show the details of the radio light curve for all VLA observing sessions in an expanded time scale. These plots have been obtained using the AIPS task DFTPL and each point corresponds to an average of 30 seconds.

### 9.3 Micro-flares variability analysis results

All panels in Figure 9.1 show that the flux density of LS I+61°303 changes significantly during typical time scales of  $\sim 1$  h or even less. Using non-relativistic causality arguments, this places an upper limit of  $\sim 10^{14}$  cm to the size of the emitting region. This value is fully consistent with source sizes of a few  $10^{13}$  cm derived from VLBI observations (Taylor et al. 1992; Massi et al. 1993; Chapter 4 of this work) and supported by outburst modeling based on particle injection into expanding plasmons (Paredes et al. 1991).

The largest amplitude variation observed took place on 1993 September 9, when the LS I+61°303 flux density changed from 131 mJy to 76 mJy in  $\sim 7$  hours. In

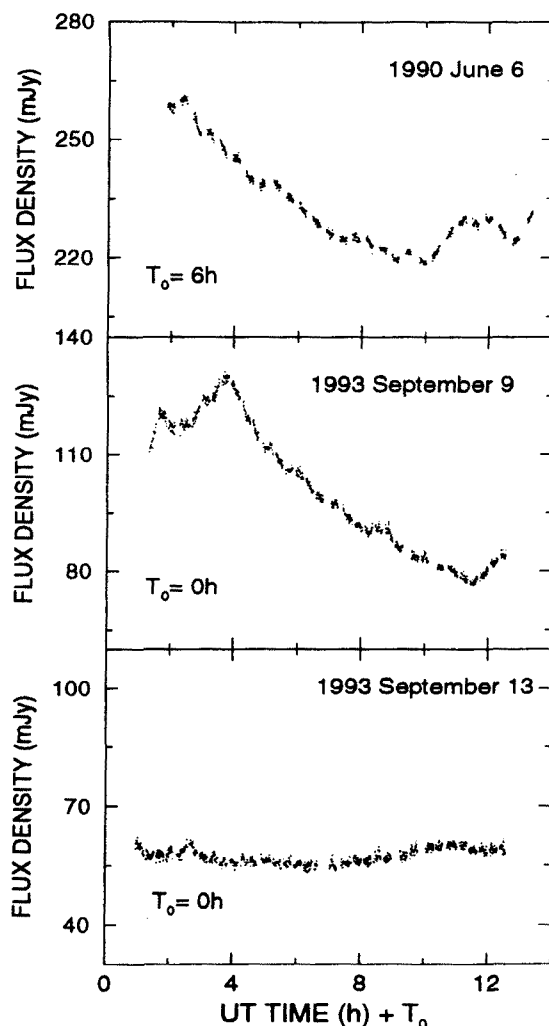


Figure 9.1: Radio light curves of LS I+61°303 as observed with the VLA with time resolution of 30 seconds. From top to bottom, the plots correspond to the observing sessions of 1990 June 6, 1993 September 9 and 1993 September 13, respectively. The rms of each data point is usually 1 mJy or less.

fact, the general trend of the data on that day does not rule out that we caught the peak of one of the strong radio outbursts, at radio phase 0.65. For the other two sessions, the total variation was much less dramatic and did not exceed 20% in a time scale of  $\sim 10$  h. It is noticeable that a simple eye inspection of the curves at the two top panels of Figure 9.1 strongly suggests that some sort of micro-flares could be superimposed on the general trend of the radio light curve, and at more or less regularly spaced time intervals.

As such micro-flares appear to be clearly active on 1993 September 9, we will first concentrate our attention on this observing session. In order to confirm a possible periodicity of the micro-flares, we removed the long-term trend of the data

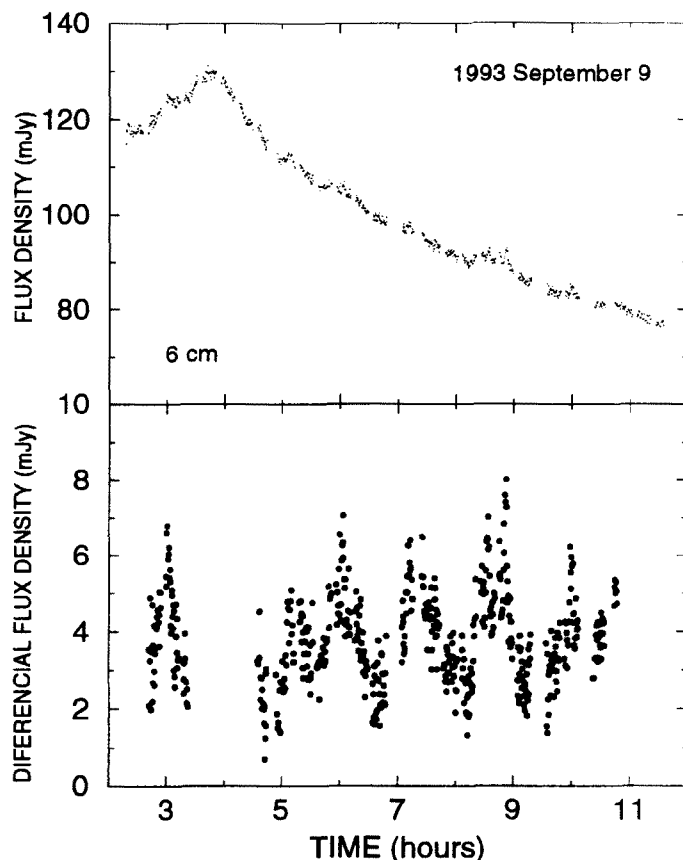


Figure 9.2: The bottom panel shows the rectified 6 cm radio light curve of LS I+61°303 resulting from the subtraction of a baseline fit in the September 9 data (which is shown in the top panel). The occurrence of micro-flares with mJy amplitude is clearly evident. To avoid possible confusion or overlap of the light curve peak with one of the micro-flares we do not use the data around 4 h UT.

by subtracting from each point the average flux density of the neighboring points within a window of 1 h length. The rectified radio light curve obtained is shown in Figure 9.2. Here the presence of micro-flares is clearly enhanced. Their amplitude is  $\sim 4$  mJy, equivalent to about 4% of the total flux density. Averaging windows between 0.5 and 1.5 hours were also applied to the data. Finally we chose it to be 1 hour length as a compromise between a too high degree of smoothing and the preservation of data points in the tails of the curve.

We used the rectified radio light curve in Figure 9.2 to search for periods in the range from one minute to a few hours. The methods used in this search were CLEAN, as adapted by Roberts et al. (1987) to time series analysis, phase dispersion minimization (PDM) method by Stellingwerf (1978) and the classical method of autocorrelating the data series. From the periodograms of Figure 9.3, we see that the three methods indicate the presence of a possible period  $P = 1.4$  h. The periodograms also show significant power at harmonics of  $P/2$  and  $2P$ .

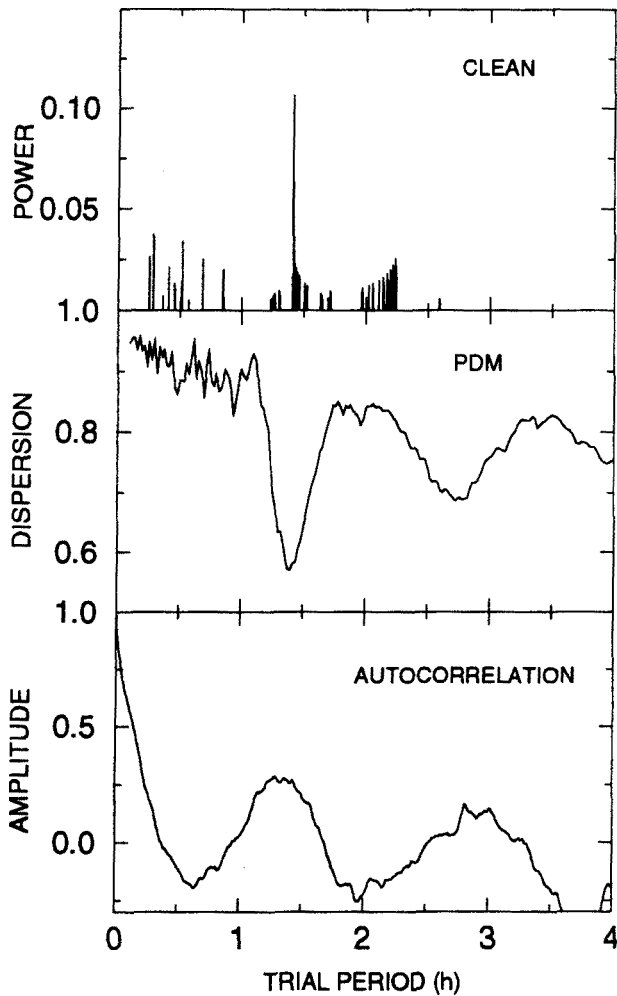


Figure 9.3: Results of the periodicity searches using the CLEAN (top), PDM (center) and autocorrelation (bottom) methods applied to the observations of 1993 September 9. All three techniques show evidence for possible underlying period at 1.4 h.

In Figure 9.4 we show the mean radio light curve obtained by folding the 1993 September 9 data with the 1.4 h period. The amplitude of the mean micro-flare is  $\sim 2$  mJy. The mean curve of each individual flare does not show a specific repeatability in the structure of the profile of the micro-flares.

A similar period analysis was also carried out for the radio light curves of 1990 June 6 (radio phase 0.72) and 1993 September 13 (radio phase 0.81). In the periodograms of the 1990 data, the same harmonics as those of the 1993 September 9 data were found although its significance in front of other peaks was not dominant. We think this is not surprising because, as it is noticeable in Figure 9.1, the data from the source during the 1990 June 6 run features regular significant gaps. This

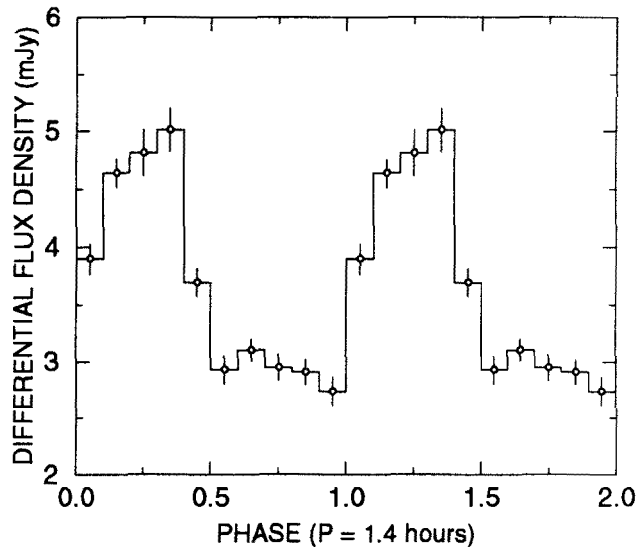


Figure 9.4: Mean 6 cm radio light curve of LS I+61°303 in 1993 September 9 obtained by folding the data with the 1.4 h period. The data have been averaged every 0.1 phase and plotted twice. The error bars represent the formal estimate of the statistical uncertainty of the mean within each bin.

fact makes less reliable both the baseline fit to the 1990 June 6 data as well as the results of period search from them. The period analysis of the 1993 September 13 light curve shows no evidence of recurrent micro-flares.

Therefore we think that as a result of this analysis *we have detected radio micro-flares with an amplitude of  $\sim 4$  mJy and a possible recurrence period of  $\sim 1.4$  hours in LS I+61°303*. The micro-flares were observed to be continuously active during  $\sim 8$  h but only when the source was *decaying from a bright level*, possibly the peak of the radio outburst.

In the next section we discuss a possible interpretation of both the presence of micro-flares around the phase of the radio outburst peak and their absence in later phases.

## 9.4 Discussion of micro-flares

We have already indicated that previous observations by Gregory et al. (1979) found neither evidence for any hourly periodic behaviour in their high time resolution radio

data nor any significant variations on time scales shorter than half an hour. We note, however, that the rms noise in the data of Gregory et al. (1979) was higher than the amplitude of the detected micro-flares and that the radio phase interval covered by their observations (0.2-0.6) was different from ours. In contrast, from the observations reported here, we think that evidences of hour scale radio periodicity may be present in general in the early decay of the LS I+61°303 radio outbursts. This is particularly clear in our 1993 September 9 data.

It is not unusual for REXRBs to exhibit radio variability on time scales of a few hours, even to a few minutes, as in the case of the possible black hole system GRS 1915+105 (Rodríguez & Mirabel 1996a). However, it is less often that this variability on time scales much shorter than the orbital period turns out to be periodic or quasi periodic. A few examples known so far include the X-ray transient source GS 2023+338, which has shown sinusoidal radio variations with periods in the range 22-120 minutes as it slowly decayed with an optically thick synchrotron spectrum (Han & Hjellming 1992). There has been also detection of flux density oscillations in the low level emission of GRS 1915+105, with periods of a few tens of minutes and amplitude changes by a factor of two (Pooley 1995; Rodríguez & Mirabel 1996b).

Based on analogy with extragalactic sources, Han & Hjellming (1992) interpreted the short term radio variability of GS 2023+338 in terms of surface brightness fluctuations caused by shock events at the ends of jets. The possibility that these hour range periods could reflect the rotation period of a neutron star does not seem very likely because they appreciably exceed that of the slowest X-ray pulsars known. Another possibility could be a hot spot in keplerian rotation around the compact object, as recently proposed by Rodríguez & Mirabel (1996b) to explain the remarkably smooth sinusoidal oscillations observed by them in GRS 1915+105. However, we believe that the lack of smoothness in the LS I+61°303 micro-flares is more consistent with a Han & Hjellming (1992) shock event interpretation than with a rotation mechanism.

In LS I+61°303, the outburst decay has an optically thin synchrotron spectrum. Therefore, in contrast with GS 2023+338, the LS I+61°303 short term radio variability should reflect actual variations in the radio source relativistic electron content rather than just surface brightness effects. Nevertheless, if models based on supercritical accretion are correct, we tentatively suggest that micro-flares during the decay of the strong LS I+61°303 radio outbursts could still be attributed as well to



shock events accelerating fresh energetic particles. It is our assumption here that, shortly after the synchrotron emitting plasmon responsible for the main outburst has been generated, secondary LDSs may possibly continue to take place for as long as supercritical accretion conditions still persist.

To see if a LDS scenario would be consistent with the observations, we must first consider two points: (i) what is the typical rise time of the main radio outburst and (ii) what is the possible duration of the supercritical accretion phase beyond that rise. The radio outburst rise time in LS I+61°303 is usually observed to be  $\sim 2$  d (Paredes et al. 1991; Estalella et al. 1993). The supercritical accretion duration is more difficult to estimate, but according to Martí & Paredes (1995) it may well last for about 0.1 radio phase interval even for highly eccentric orbits, i.e., possibly larger than the rise time. So once the first and possibly more energetic shocks have traveled beyond the binary system volume in  $\sim 2$  d and build up the radio emitting plasmon at scales of a few  $10^{13}$  cm, supercritical accretion still may persist allowing secondary LDSs to occur. However, as the accretion rate tends now to decrease with time, these later shocks will produce less energetic radio flares, which we identify with the observed micro-flares during September 9 (phase  $\sim 0.66$ ). This picture is furthermore in agreement with the fact that Figure 9.1 shows that micro-flares were later absent on September 13 (phase  $\sim 0.81$ ), when supercritical accretion was probably no longer occurring.

We may use the simple formulation of Haynes et al. (1980) and TG84 for LDSs in order to gather some further physical insight. These authors assumed spherically symmetric supercritical accretion at a rate  $\dot{M}_{\text{acc}}$  onto a neutron star of mass  $M_c$  with a free-fall density law  $\rho(r) = \Lambda r^{-3/2}$ , where  $\Lambda = \dot{M}_{\text{acc}}/4\pi\sqrt{2GM_c}$ . For a blast wave of the form described by Sedov (1959), the shock radius will travel radially as a function of time according to  $R = (E/\Lambda)^{2/7}t^{4/7}$ , where  $E$  is the energy injected into the blast. In our case, the time separation between micro-flares is  $\Delta t \simeq 1.4$  h. If we roughly interpret this as a free-fall time, the corresponding distance of the accreting matter reservoir from a  $1 M_\odot$  neutron star is  $r_{\text{ff}} \simeq 1.4 \times 10^{11}$  cm, considerably smaller than the periastron separation. Then, for an accretion rate higher but close to its Eddington limit ( $\sim 2 \times 10^{-8} M_\odot \text{ yr}^{-1}$ ) and plausible blast energies of  $10^{39}$ - $10^{41}$  erg, the shock front is able to clear the volume limited by  $r_{\text{ff}}$  in  $10^1$ - $10^2$  s, i.e., consistently shorter than  $\Delta t$ .

If supercritical accretion does not occur in LS I+61°303, we should try to interpret

the micro-flares in the context of the alternative models where the LS I+61°303 radio outbursts are the result of the interaction between the normal wind from the primary and the relativistic wind from the neutron star (Maraschi & Treves 1981; Lipunov & Nazin 1994). It is possible that some sort of oscillation in the wind boundaries could cause the micro-flares but this is possibly a much more complicated problem.

It may be expected from the LDS interpretation that micro-flares in the radio should likely be preceded by nearly coincident micro-flares in X-rays, with the same 1.4 h period. Unfortunately, the X-ray published so far do not have sampling times with enough resolution to search for such a short period or its signal to noise ratio is too low to emphasize a possible small brightness amplitude. (see description of the LS I+61°303 ASM data in next chapter). Additional X-ray high timing resolution observations would be required to test this idea.

# Bibliografy

- [1] Estalella R., Paredes J.M., Rius A., Martí J., Peracaula M., 1993, A&A, 268, 178
- [2] Gregory P.C., Taylor A.R., Crampton D., Hutchings J.B., Hjellming R.M., et al., 1979, AJ, 84, 1030
- [3] Han X., Hjellming R.M., 1992, ApJ, 400, 304
- [4] Haynes R.F., Lerche I., Murdin P., 1980, A&A, 87, 299
- [5] Lipunov V.M., Nazin S.N., 1994, A&A, 289, 822
- [6] Maraschi L., Treves A., 1981, MNRAS, 194, 1
- [7] Martí J., Paredes J.M., 1995, A&A, 298, 151
- [8] Massi M., Paredes J.M., Estalella R., Felli M., 1993, A&A. 269, 249
- [9] Paredes J.M., Martí J., Estalella R., Sarrate J., 1991, A&A. 248, 124
- [10] Pooley G., 1995, IAU Circ. 6269
- [11] Roberts D.H., 1995, IAU Circ. 6269
- [12] Rodríguez L.F., Mirabel I.F., 1996a, in *Radio Emission from the Stars and the Sun*, A.R. Taylor & J.M. Paredes
- [13] Rodríguez L.F., Mirabel I.F., 1996b, ApJ Letters (submitted)
- [14] Sedov L., 1959, *Similarity and Dimensional Methods in Mechanics*, New York, Academic Press
- [15] Stellingwerf R.F., 1978, ApJ, 224, 953

[16] Taylor A.R., Gregory P.C. 1984, ApJ, 283, 273 (TG84)

[17] Taylor A.R., Kenny H.T., Spencer R.E., Tzioumis A., 1992, ApJ, 395, 268

# Chapter 10

## Search for X-ray periodicity in LS I+61°303

### 10.1 Introduction

X-ray variations have been detected in a large amount of the about 200 X-ray binaries identified. Several groups of this kind of sources have been able to be classified through their X-ray variability behaviour and this helps to better understand the physics of each particular system.

Different variability patterns encountered in the X-ray binary population are for example:

- variations linked to the orbital period (like low-mass X-ray binaries –dipping sources–),
- transient sources (some recurrent and among them some periodically recurrent),
- type I bursts and type II bursts,
- pulsars and among them milli-second pulsars,
- quasi-periodic oscillations,
- irregular variations,
- third periods and beating periods.

LS I+61°303 has been during years a source very seldomly observed at X-rays, and up to recently not much was known about its time behaviour in this range of the wave energy spectrum.

The first detection of X-ray photons from LS I+61°303 was published by Bignami et al. in 1981. These authors reported the source to be constant within a 30% of a flux level of  $2 \times 10^{-12}$  erg cm<sup>-2</sup> s<sup>-1</sup>; however, they were based on only two data points taken several orbital cycles apart. Goldoni & Mereghetti (1995) reported a variation of a factor of 3 over a time scale of few days, with an average X-ray flux of  $4 \times 10^{-12}$  erg cm<sup>-2</sup> s<sup>-1</sup>.

The first detected X-ray outburst of LS I+61°303 has been presented in Chapter 3 of this work and was published by Taylor et al. (1996). We remind here that these ROSAT X-ray observations of LS I+61°303 were coordinated with VLA radio observations and carried out over one orbital cycle in August–September 1992. The unabsorbed X-ray luminosity derived for that occasion was of about few times  $10^{34}$  erg s<sup>-1</sup> in the 0.1–2.4 keV range. The lapse of time of X-ray activity was of about 10 days, similar to the radio outbursts.

The few days time scale variability and flaring behavior already seen in X-rays by ROSAT, clearly suggested the possibility that LS I+61°303 could also undergo periodic X-ray outbursts in connection with the periodic radio emission. In order to check this suspicion, a long term continuous X-ray monitoring of LS I+61°303 should be necessary beyond the few pointed observations so far available in the literature. In this context, the existence and public availability of quick-look results provided by the team of the All Sky Monitor (ASM) on board the Rossi X-Ray Timing Explorer (RXTE) appear as a plausible source of data to search for the suspected X-ray period of LS I+61°303. The sensitivity of LS I+61°303 data from the ASM/RXTE is not good enough to provide a detailed monitoring of individual X-ray outbursts from cycle to cycle. However, the huge amount of ASM data available is likely to compensate for the lack of sensitivity when folded and averaged on the correct X-ray period. Up to now, the ASM data for LS I+61°303 includes nearly ten months of daily monitoring and this is the only X-ray data from which a longterm period search can be envisaged. This search appears to be successful and we report here in detail our period detection results.

## 10.2 X-ray period search using ASM/RXTE data

The ASM/RXTE consists of three wide-angle shadow cameras all of them equipped with proportional counters. The energy range is 2–10 KeV, with a total collecting area

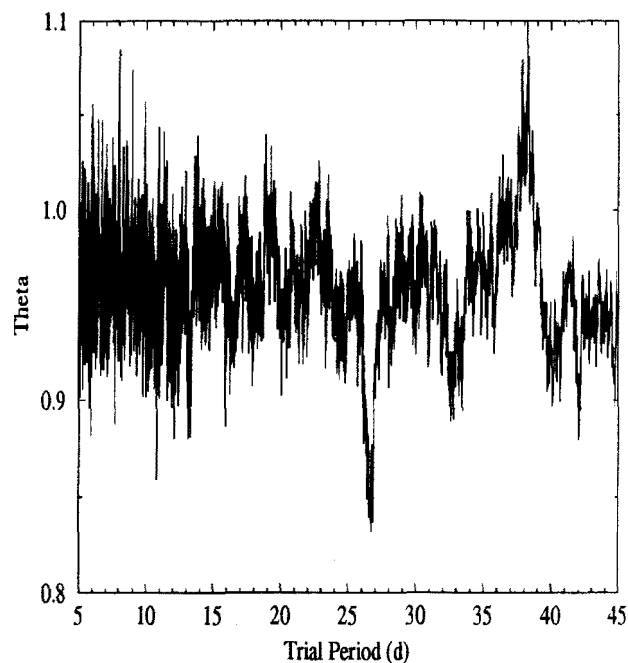


Figure 10.1: Periodogram of the ASM/RXTE daily data for LS I+61°303 using the phase dispersion minimization technique (PDM). The period search has been carried out between 5 and 45 d, and the deepest minimum found corresponds to a period of 26.7 d.

of 90 cm<sup>2</sup>. The time resolution allows to cover 80% of the sky every 90 minutes. In our period analysis, we used the daily averaged ASM data of LS I+61°303, spanning from 1996 late February to early December and amounting to 269 flux measurements. Each data point represents the one-day average of the source fluxes of individual ASM dwells, typically 5-10 fluxes per day. The error value of the daily averages corresponds to the quadrature average of the estimated errors on the individual dwells of the day.

The methods PDM and CLEAN (already described and used in previous chapters) were used to search for periodicities.

In Figure 10.1, we show the result of applying the PDM method to the ASM data in the period range 5-45 d. The most significant minimum was found at a period of  $26.7 \pm 0.2$  d. This result is independently confirmed when using the CLEAN method. The CLEAN power spectrum, displays a clear component power at a nearby but slightly larger period. The fact that a very similar period is found after applying two independent methods gives us confidence about reality of the X-ray period detection.

At this point, it is remarkable that *the X-ray period of  $26.7 \pm 0.2$  days we have found is consistent with the radio period of  $26.71 \pm 0.05$  days we have determined in Chapter 8* by using a approximately two years span of LS I+61°303 data from the daily monitoring program of the Green Bank Interferometer. An independent analysis using Green Bank data by Ray et al. (1996) yields a period of  $26.69 \pm 0.02$ . However the X-ray period here found is also well consistent within error with the  $26.496 \pm 0.008$  d radio period, as determined by Taylor & Gregory (1984) using more than a decade old observations. It is not clear at present time if the last results for the radio and X-ray periods of about 26.7 days represent a real increase related to orbital period change or some other effects are at work. The X-ray period detected by us is not accurate enough to support a longer radio period value, but it is certainly consistent too with any of the recent longer radio period estimates. Independently of any period evolution, the closeness within error of the LS I+61°303 X-ray and radio periods strongly suggests that they are actually the same.

Hereafter, and for practical computation purposes, we will fold the ASM data using our 26.7 d X-ray period value. Also, we will adopt always the same phase origin at JD 2443366.775, as originally set by Taylor & Gregory (1982).

The X-ray light curve, folded and averaged in bins of 0.1 phase, is shown in the bottom panel of Figure 10.2. In the top panel of this same figure, we plot for comparison purposes an average radio light curve at 8.4 GHz. This radio light curve has been obtained by averaging three different radio outbursts taken from Tavani et al. (1996). The data are folded twice for better representation of the cycle.

The value assigned to each bin in the folded X-ray curve is the weighted average of about 25 ASM points. Given that this is a relatively high number, we regard the X-ray folded and averaged light curve as significant at least concerning its general shape, but possibly not the details. Representative error bars computed as the weighted error of the averaged bin mean are also indicated.

### 10.3 Discussion

The overall shape of the average X-ray light curve shown in Figure 10.2 is noticeably different from that seen in the radio. X-ray emission is wider and spans longer than high radio emission, with a common overlap in the active state around phases 0.6-



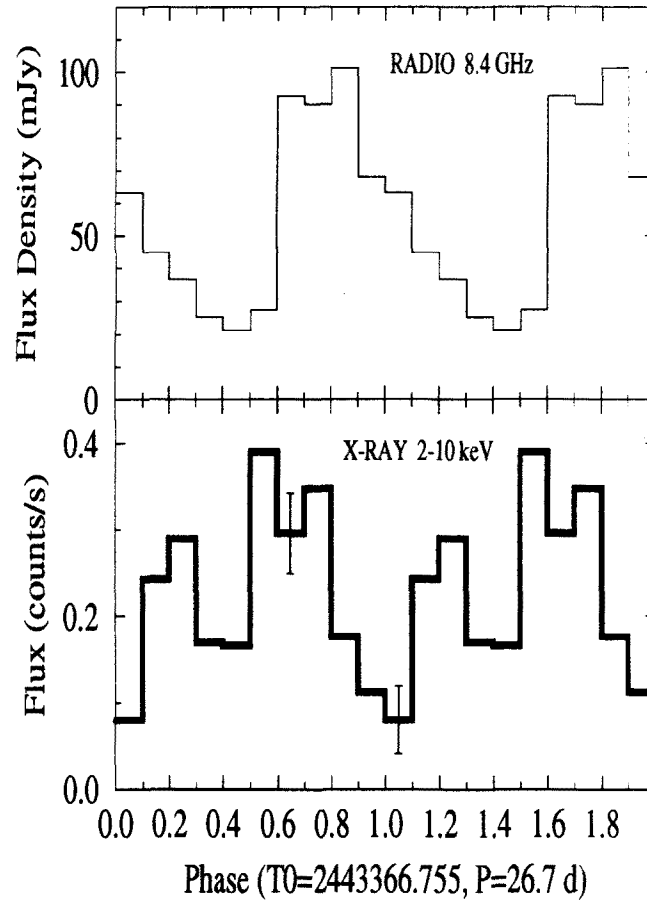


Figure 10.2: **Bottom:** ASM/RXTE observations of LS I+61°303 in the 2-10 keV band folded on the 26.7 d period and averaged in bins of 0.1 phase. Representative error bars are shown. **Top:** Averaged radio light curve at 8.4 GHz folded on the same period as the X-ray data. The phase origin adopted corresponds to JD 2443366.775 in both panels and all data points are plotted twice.

0.8. The X-ray emission level from LS I+61°303 appears to vary by a factor of  $\sim 5$ , with a broad active state that lasts for more than half an X-ray period and is centered around phase 0.5. A rather narrow X-ray minimum appears to be present at phases 0.9-0.1 and the X-ray light curve may also exhibit two maxima with different amplitude. This last point, however, should be confirmed from less noisy X-ray data.

Although we do not have spectral X-ray information, we can try to derive a rough estimate of the LS I+61°303 2-10 keV luminosity range knowing that the ASM Crab Nebula count rate in this energy band is  $\sim 75$  ASM counts  $s^{-1}$ . From the LS I+61°303 count rate, the corresponding luminosity at a distance of 2.0 kpc (Frail & Hjellming 1991) is then found to vary within  $L_X(2-10 \text{ keV}) \sim 1 \times 10^{34}$  and  $\sim 6 \times 10^{34}$  erg  $s^{-1}$ . This range is consistent in order of magnitude with the X-ray luminosities observed by other authors (e.g. Taylor et al. 1996). Our luminosity estimates are not corrected for absorption due to the atomic hydrogen column density. Frail & Hjellming (1991) HI observations yielded  $N_H = 8.4 \times 10^{21}$   $\text{cm}^{-2}$  for LS I+61°303. Therefore, the absorption correction should not be larger than about 10% in the ASM energy band.

In the full cycle simultaneous X-ray and radio analysed in Chapter 3 we saw that X-ray and radio maxima occurred at well separated phases, and the X-ray flux varied by a factor of  $\sim 10$ . This fractional variability is higher but comparable to the averaged one we have found in the present study. The average light curves from the XTE data display significant X-ray emission preceding the onset of the radio outburst as in the case of the outburst observed in 1992.

Since both X-ray and radio emission appear to display the same periodicity, this implies that any model explaining the radio outbursts should also take into account, and be consistent with, the concurrent X-ray emission of the system. Current models proposed so far can be divided into two main broad categories, namely, accretion models and those based on a young non-accreting pulsar.

Accretion models initially proposed assumed that relativistic electrons were ejected and accelerated after super Eddington accretion events of mass from the Be star circumstellar envelope onto the neutron star companion surface (e.g., Taylor et al. 1992). This was supposed to occur during the periastron passage of a highly eccentric orbit. Recent X-ray observations by the ASCA satellite (Harrison et al. 1997) provide strong evidence that this scenario needs to be revised. In particular, the ASCA observations indicate a non-thermal power law spectrum together with an

X-ray luminosity at least three orders of magnitude lower than predicted for super Eddington accretion. In addition, no X-ray pulsations nor Fe line features in the X-ray spectrum have been ever detected. A possible, but difficult, way to overcome this problem would be if the bulk of energy was emitted in the  $\gamma$ -rays rather than in the X-ray regime, possibly involving a photon shift towards higher energies due to inverse Compton emission. Another alternative is to consider that the accretion takes place over the magnetosphere of a rapidly rotating magnetized neutron star (Campana et al. 1995).

On the other hand, non-accretion models involve a relatively young pulsar in a binary system. The radio outbursts are then originated from particles accelerated at the shock front produced at the interface between the dense Be star wind and the relativistic wind of the pulsar (Maraschi & Treves 1981; Tavani 1994). Synchrotron and inverse Compton emission of the same particles may also account for the X-ray emission of the system and perhaps  $\gamma$ -ray too. Both the X-ray and radio light curves are expected here to be modulated with the orbital period as the shock geometry changes along the orbit.

Concerning the origin of ASM X-rays, the fact that the highest X-ray and radio emission states take place roughly at the same orbital phases (0.6-0.8) could suggest that there is an important X-ray component produced by inverse Compton effect over the radio emitting electrons. Such production of non-thermal X-rays in the keV band is more naturally understood in the framework of non-accreting models since accretion X-rays would tend to produce a rather thermal spectrum.

## 10.4 Conclusions

Based on ASM/RXTE quick look data, we find significative evidence of an X-ray period of  $26.7 \pm 0.2$  d for the radio emitting X-ray binary LS I+61°303. *The X-ray period appears to be the same as the radio/orbital period of the system.* This fact gives support to the idea that the X-ray and radio emission of LS I+61°303 are strongly related.

Given the ASM sensitivity and the weak X-ray flux of LS I+61°303, the X-ray light results presented here have been necessarily based on averaging many orbital cycles of ASM data. Therefore, further coordinated radio and higher sensitivity X-

ray observations of individual outbursts are needed in order to better understand the relationship between these two spectral domains suggested by the existence of a common period.

The averaged X-ray light curve obtained displays a broad active state whose highest emission level overlaps with the phases of strongest radio emission. This could be interpreted as inverse Compton effect playing an important role in the production of X-rays, as assumed in the scenario modeled in Chapter 2 of this report.

# Bibliografy

- [1] Bignami G.F., Caraveo P.A., Lamb R.C., Markert T.H., Paul J.A., 1981, ApJ, 247, L85
- [2] Campana S., Mereghetti S., Colpi M., Stella L., 1995, A&A, 297, 385
- [3] Frail D., Hjellming R.M., 1991, AJ, 101, 2126
- [4] Goldoni P., Mereghetti S., 1995, A&A, 299, 751
- [5] Harrison F.A., Leahy D., Waltman E., 1997, ApJ (submitted)
- [6] Maraschi L., Treves A., 1981, MNRAS, 194, 1
- [7] Peracaula M., 1997, PhD Thesis, University of Barcelona
- [8] Ray P.S., Foster R.S., Waltman E.B., Ghigo F.D., Tavani M., 1996, ApJ (submitted)
- [9] Tavani M., 1994, in *The Gamma-Ray Sky with GRO and SIGMA*, Dordrecht: Kluwer, 181
- [10] Tavani M., Hermsen W., van Dijk R., et al., 1996, A&ASS, 120, 243
- [11] Taylor A.R., Gregory P.C. 1982, ApJ, 255, 210
- [12] Taylor A.R., Gregory P.C. 1984, ApJ, 283, 273
- [13] Taylor A.R., Kenny H.T., Spencer R.E., Tzioumis A., 1992, ApJ, 395, 268
- [14] Taylor A.R., Young G., Peracaula M., Kenny H.T., Gregory P.C., 1996, A&A, 305, 817



# Chapter 11

## Search for radio periodicity in Cygnus X-3

### 11.1 Introduction

The X-ray variations of the High Mass X-ray Binary System Cygnus X-3 are known since long to be clearly regular with a period of 4.8 hours (Parsignault et al. 1976). This X-ray flux modulations are thought to be coincident with its orbital period.

At radio wavelengths the source displays a periodical recurrent strong non-thermal outbursts (Gregory et al. 1972), during which it shows a jet-like morphology (Geldzahler et al. 1983; Spencer et al. 1986).

Outside the periods of major outbursts, Cygnus X-3 normally shows quiescent variable radio emission at the level of 50 to 500 mJy (Hjellming & Balick 1972; Mason et al. 1976). Molnar et al. (1984) suggest that this emission is produced by continuous superposition of low-amplitude radio flares similar in nature to, but weaker than, the major outbursts. On the basis of a cross-correlation study of the shape of series of flares in independent observations Molnar (1985) also suggests that there is a significant recurrence of the low level radio outbursts with a period of 4.95 hours, similar to the orbital period of 4.8 hours. However, the significance of this radio period is limited due to the short data base involved in the analysis and the complex structure of the different flares. In addition, this periodic component was not confirmed in a radio monitoring by Johnston et al. (1986) carried out at the

end of a major burst.

Long-term periodic variations of 17 d, 33 d and 34 d in the X-ray flux of the source have been reported by several authors, and explained as due to the effects of precession, eccentricity of the orbit, or apsidal motion, but none of these periods has been confirmed by more extensive observations (Bonnet-Bidaud & Chardin 1988).

In order to study the possible short periodicity at radio wavelengths, we started a program of radio observations of Cygnus X-3. We now present the observations of the source obtained in our campaign and the results of the period analysis on these data.

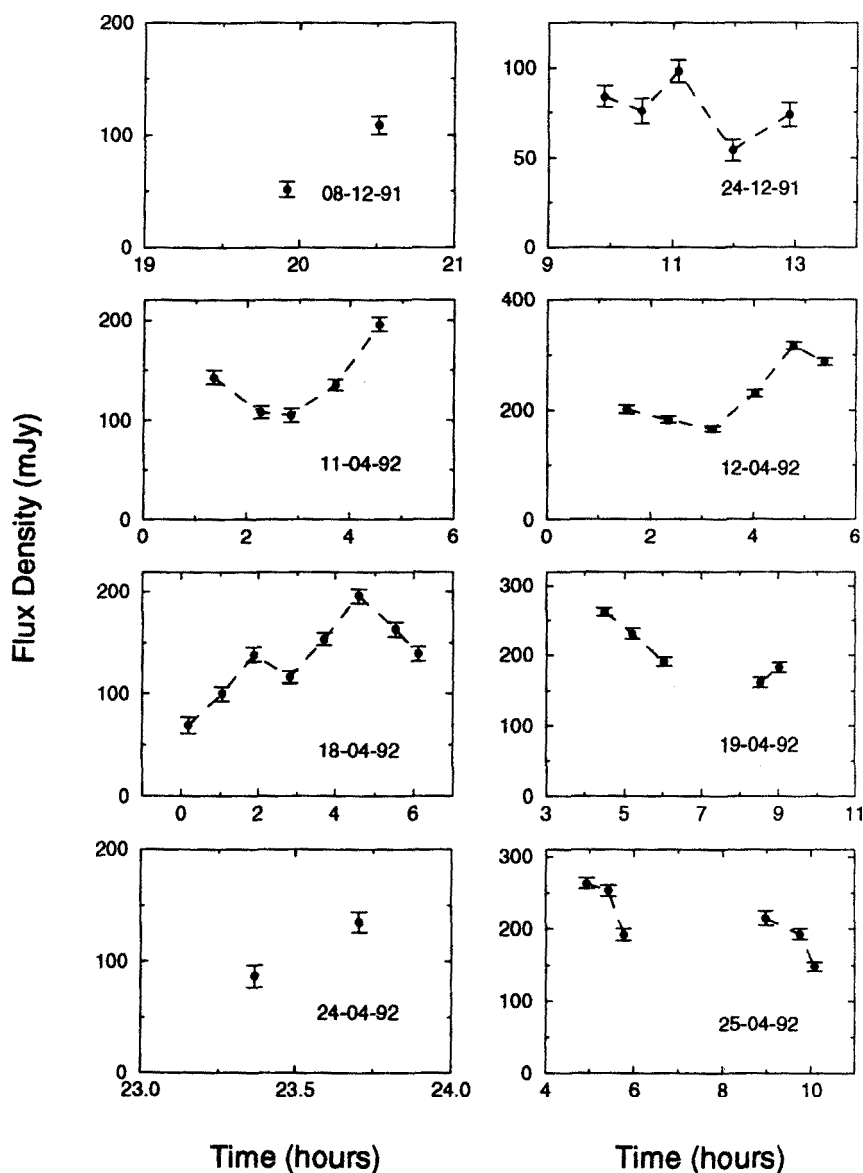


Figure 11.1: Flux density at 3.6 cm wavelength plotted as a function of time for December 1991–Apr 1992 data. Errors on individual measurements are less than 10%.



## 11.2 Observations

The observations were carried out with the 70 m antenna at the Madrid Deep Space Communication Complex (INTA-NASA) at 3.6 cm wavelength (8.4 GHz). Right and left circular polarizations were observed simultaneously using a dual band reflex-feed system (Rusch 1976) at the antenna secondary focus, a dual-channel Noise Adding Radiometer and a special antenna control system (Rius et al. 1988).

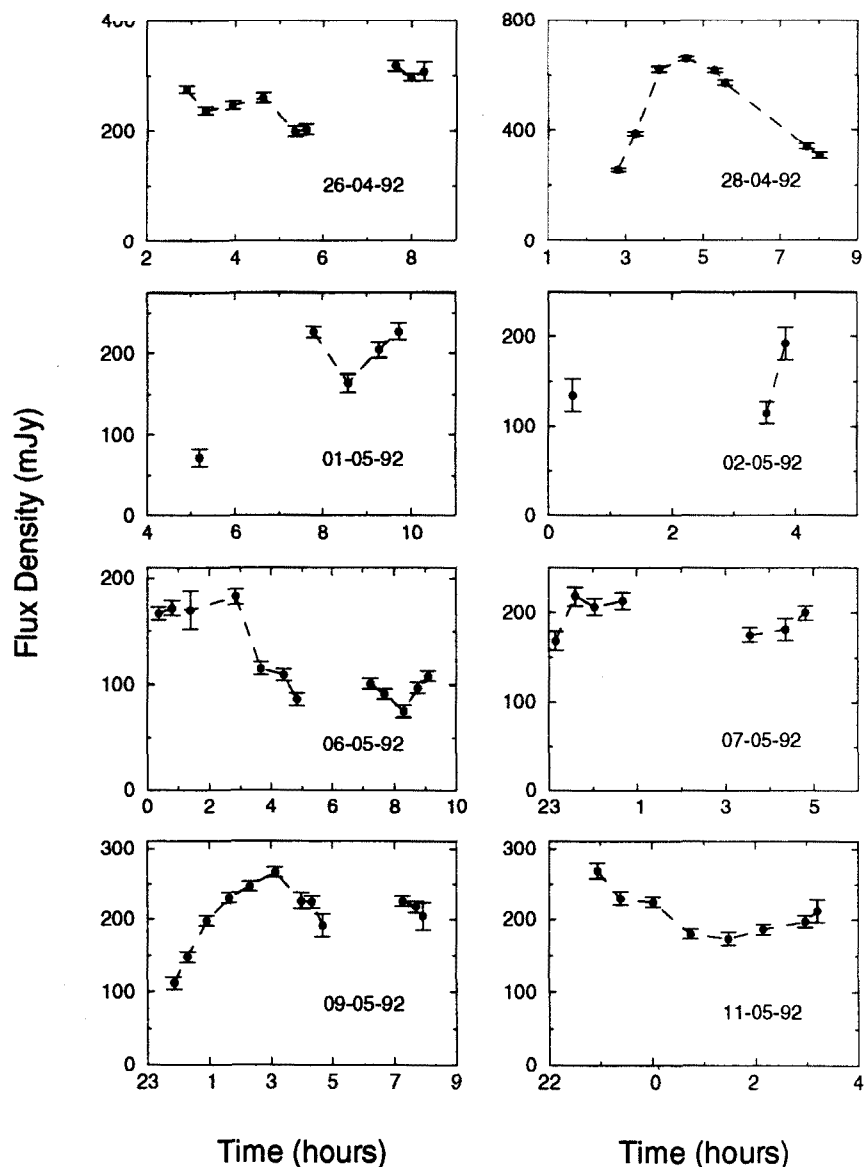


Figure 11.2: Flux density at 3.6 cm wavelength plotted as a function of time for Apr 1992–May 1992 data. Errors on individual measurements are less than 10%.

Each measurement consists of ten scans of two minutes each at a constant hour angle in order to minimize elevation and atmosphere dependence of system temperature. After rejecting scans with noise interference or bad data, an estimation of the flux density of the source was obtained by fitting a gaussian curve to the average of the scans. In order to check the telescope pointing and calibration, each observing sequence on Cygnus X-3 was preceded and followed by the observation of the calibration source DR 21, for which we assumed a peak flux density of 21.43 Jy at 8.4 GHz. Further details of the observing technique are reported in Paredes et al. (1987, 1990). The data were reduced using the standard software-packages available at the telescope site (Rius et al. 1988).

We carried out a total of 16 observing sessions, distributed from December 1991 to May 1992, obtaining a total of 104 measurements of the flux density of Cygnus X-3. Figures 11.1 and 11.2 show the flux density profile obtained during all the observing sessions. The estimated error of each point is less than 10%.

### 11.3 Data reduction

As it can be seen in Figures 11.1 and 11.2, the observed radio emission consists of low-level radio flares with a short time scale variation. The emission level, except for the flare observed on April 28, is less than 400 mJy, which is characteristic of the quiescent radio emission of Cygnus X-3 (Mason et al. 1976; Molnar et al. 1984). The data corresponding to the April 28 flare were not used in the period analysis.

To search for periodicity in the quiescent radio emission of Cygnus X-3 we used the two methods CLEAN and PDM described in Chapter 7.

#### 11.3.1 CLEAN algorithm

The application of the CLEAN algorithm to our data is shown in Figure 11.3, in which the Direct Fourier Transform power spectrum and CLEAN components are plotted. The main peak present in the CLEAN components, after 100 iterations, was found at the frequency of 1.144 cycles/d, corresponding to a period of 20.98 h. The spectral window for the same data presents a significant peak at the frequency

of 1.002 cycles/d, due to gaps in data sampling. For the frequency of 1.144 cycles/d, the spectral window does not show any significant peak.

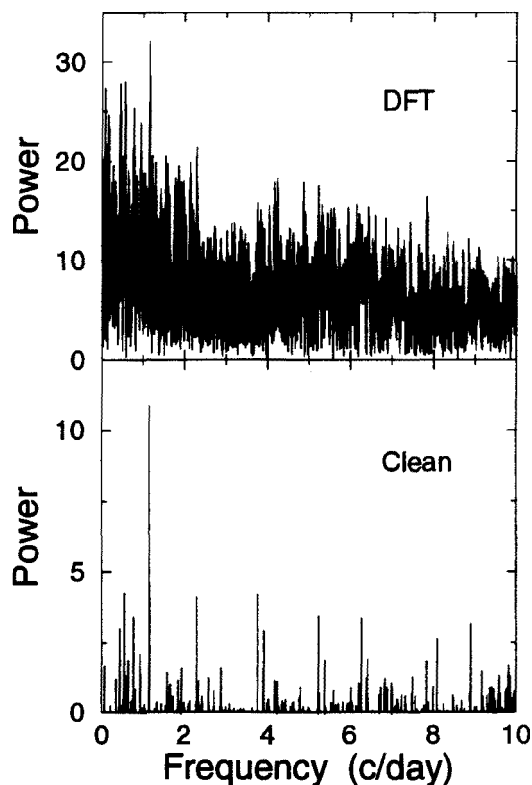


Figure 11.3: DFT power spectrum (top) and CLEAN components (bottom). The highest CLEAN component has a frequency of 1.144 cycles/d.

Tests were carried out in order to assess the reliability of our results. Multiperiodic data, with different amplitudes superimposed to gaussian noise, were synthesized with the same sampling as the actual observations. The CLEAN algorithm was able to identify the frequencies present in the data correctly. Another test performed was to divide our data set in two parts (April and May) and apply the analysis to each part independently. The same frequency of 1.144 cycles/d was obtained for each data set.

### 11.3.2 Phase dispersion minimization method

The result of the PDM analysis of our data is shown in Figure 11.4. The most significant minimum corresponds to a period of 0.869 d (20.86 h), which agrees very

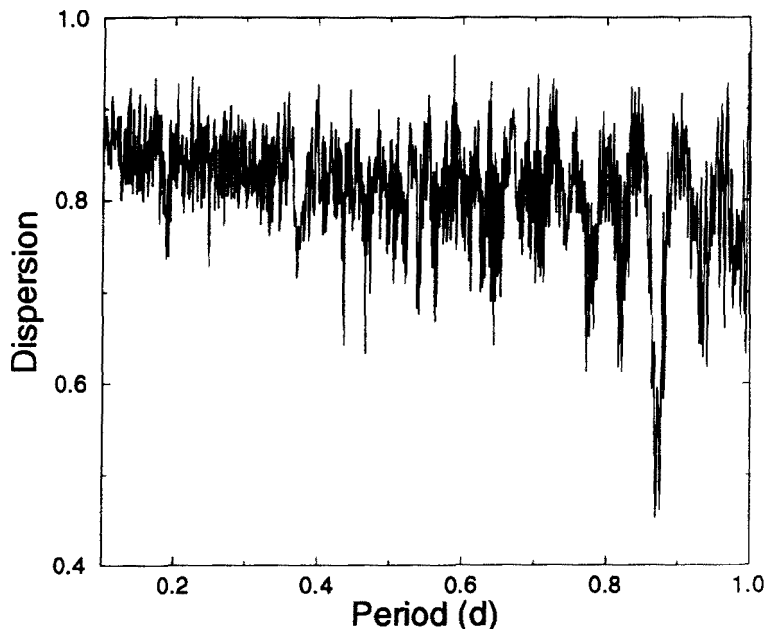


Figure 11.4: PDM periodogram of the original data obtained during the quiescent state of Cygnus X-3. The minima corresponds a period of 0.869 days. The bin structure is (5,2) and the temporal step 0.001 day

well with the period determined using the CLEAN algorithm. The method was also applied to the data divided in two parts. A minimum for the same period of 0.869 d was obtained for each data set.

## 11.4 Results

After applying both methods to our data we found that the dominant feature is a 21 h period. In addition, the first harmonic (10.5 h) also appears in both analyses (see Figures 11.3 and 11.4) together with other minor features with a low confidence level.

In Figure 11.5 we show the light curve obtained by folding all the data points with a 20.9 h period. The horizontal axis is labeled in phase. Phase zero has been set at Julian Date 2440949.889, epoch corresponding to the minimum in the X-ray cycle (van der Klis et al. 1981). The continuous curve represents the results of a least-square sine-wave fit to the data:

$$S = A_0 + A_1 \sin[2\pi(\phi + \phi_0)] \quad (11.4.1)$$

where  $S$  is the flux density and  $\phi$  the phase. The fitted values are:  $A_0 = 176.4$  mJy,

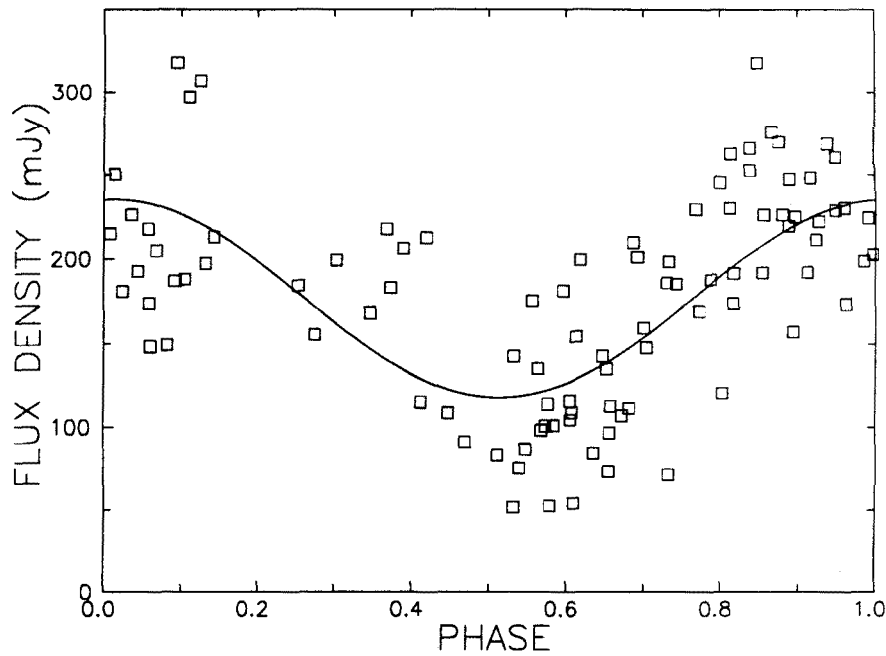


Figure 11.5: Radio light curve of the data obtained by folding the measurements taken between December 1991 and May 1992 with the 20.9 hour period. The continuous curve is the result of a least-square sine-wave fit to the data

$A_1 = 58.8$  mJy, and  $\phi_0 = 0.23$ .

As it can be seen in Figures 11.3 and 11.4, no significant period is found in the range 4.8-5.1 h, and we cannot confirm the 4.95 h period claimed by Molnar et al. (1984).

The analysis of our data seems indicate that the low level flares, with a duration of few hours, are affected by a modulation of 20.9 h with a peak-to-peak amplitude of  $\sim 120$  mJy. This 21-hour period is shorter than those found in the different energy regions, and should be confirmed by more extensive observations.



# Bibliografy

- [1] Bonnet-Bidaud J.M., Chardin G. 1988, Phys. Rep. 170, 325
- [2] Geldzahler B.J., Johnston K.J., Spencer J.H. et al. 1983, ApJ 273, L65
- [3] Gregory P.C., Kronberg P.P., Seaquist E.R. et al. 1972, Nat 239, 440
- [4] Hjellming R.M., Balick B. 1972, Nat 239, 443
- [5] Johnston K.J., Spencer J.H., Simon R.S. et al. 1986, ApJ 309, 694
- [6] Mason K.O., Becklin E.E., Blankenship L. et al. 1976, ApJ 207, 78
- [7] Molnar L.A. 1985, Ph. D. Thesis, Harvard University
- [8] Molnar L.A., Reid M.J., Grindlay J.E. 1984, Nat 310, 662
- [9] Parsignault D.R., Schreier E., Grindlay J., Grusky H. 1976, ApJ 209, L73
- [10] Rius A., Chamarro A., Estalella R. et al. 1988, RA-Tools: Data Gathering System for Radio Astronomical Applications, MDSCC Madrid
- [11] Rusch W.V.T. 1976, in Methods of Experimental Physics 12. Part B, ed. M.L. Meeks, Academic Press, New York, p 29
- [12] Spencer R.E., Swinney R.W. Johnston K.J., Hjellming R.M., 1986, ApJ 309, 604
- [13] van der Klis M., Bonnet-Bidaud J.M. 1981, A&A 92, L5





TD PER

0700451992

